3386–3397 *Nucleic Acids Research, 2013, Vol. 41, No. 5* *Published online 29 January 2013*
doi:10.1093/nar/gkt008

Characterization of MicA interactions suggests a potential novel means of gene regulation by small non-coding RNAs

Charlotte A. Henderson, Helen A. Vincent, Carlanne M. Stone, Jack O. Phillips, Peter D. Cary, Darren M. Gowers and Anastasia J. Callaghan*

Biophysics Laboratories, School of Biological Sciences, Institute of Biomedical and Biomolecular Sciences, University of Portsmouth, Portsmouth PO1 2DT, UK

Received January 18, 2012; Revised December 18, 2012; Accepted December 21, 2012

ABSTRACT

MicA is a small non-coding RNA that regulates *ompA* mRNA translation in *Escherichia coli*. MicA has an inhibitory function, base pairing to the translation initiation region of target mRNAs through short sequences of complementarity, blocking their ribosome-binding sites. The MicA structure contains two stem loops, which impede its interaction with target mRNAs, and it is thought that the RNA chaperone protein Hfq, known to be involved in MicA regulation of *ompA*, may structurally remodel MicA to reveal the *ompA*-binding site for cognate pairing. To further characterize these interactions, we undertook biochemical and biophysical studies using native MicA and a 'stabilized' version, modified to mimic the conformational state of MicA where the *ompA*-binding site is exposed. Our data corroborate two proposed roles for Hfq: first, to bring both MicA and *ompA* into close proximity, and second, to restructure MicA to allow exposure of the *ompA*-binding site for pairing, thereby demonstrating the RNA chaperone function of Hfq. Additionally, at accumulated MicA levels, we identified a Mg^{2+}-dependent self-association that occludes the *ompA*-recognition region. We discuss the potential contribution of an Mg^{2+}-mediated conformational switch of MicA for the regulation of MicA function.

INTRODUCTION

In *Escherichia coli*, cellular stresses that compromise the integrity of the bacterial envelope are mediated through the σ^E pathway. This sigma factor activates the expression of genes that respond to stresses like ethanol exposure, heat shock, hyperosmotic pressure and the accumulation of mis-folded proteins. In normal conditions, σ^E is sequestered in the cytoplasmic membrane by an anti-σ factor, RseA (1,2). On exposure to extracytoplasmic stress, however, DegS and RseP proteases cleave the RseA, releasing σ^E (2,3). Consequently, >80 genes that participate in the homeostasis, synthesis and assembly of outer membrane proteins are induced (4,5).

One of the induced genes, affected in the manner outlined earlier in the text, encodes the small non-coding RNA (sRNA) MicA, which interacts with the 5′-untranslated region of specific messenger RNAs through short sequences of complementarity (6). For MicA to accommodate interaction with several mRNA targets, base pairing is often limited to an imperfect region of 10–20 nt, typically located near the ribosome-binding site of the mRNA. Interestingly, some sRNAs must be structurally remodelled to present their mRNA-interaction site, as is the case for MicA binding to its target, *ompA* (6), which encodes a protein involved in maintaining the structural integrity of the cell's outer membrane (7,8). In this way, MicA can interact with *ompA* to cause a negative regulatory effect on its translation. This results from the pairing of MicA to the translation initiation region within *ompA*, preventing its translation and making it vulnerable to degradation by RNases (6,9).

A crucial factor for efficient regulation of many mRNAs via an sRNA-mediated pathway is the Sm-like protein Hfq. This protein is highly abundant in Gram-negative bacteria and was first discovered in the 1960s as a host factor for the RNA bacteriophage Qβ, in which Hfq melted the 3′-end of the genomic RNA to improve the replication efficiency (10,11). Hfq has since been shown to aid the regulation of many sRNA-mediated

*To whom correspondence should be addressed. Tel: +44 023 9284 2055; Fax: +44 023 9284 2070; Email: anastasia.callaghan@port.ac.uk
Present address:
Helen A. Vincent, School of Chemistry and Manchester Institute of Biotechnology, University of Manchester, 131 Princess Street, Manchester, M1 7DN, UK.

pathways, although the mechanism by which this occurs is largely unknown. One proposed mechanism for regulation is that Hfq improves the likelihood of pairing by simultaneously binding both the sRNA and mRNA, thereby increasing their intermolecular proximity. The distinction of two RNA binding faces on Hfq (distal and proximal) may enable this proposed mode of action (12–14). Ternary complexes have also been visualized *in vitro* for an increasing number of sRNA–mRNA pairs, supporting the proposed mechanism (15,16). Alternatively, Hfq may alter the structure of the sRNAs, to make accessible the complementary region to its target mRNA. Restructuring of RNAs by Hfq has been described recently for the mRNAs, s*odB* and *rpoS*, and the sRNA, OxyS (17–19). Moreover, it is unknown whether Hfq provides the same role to all sRNA–mRNA pairs.

We undertook biochemical and biophysical characterization of the MicA:*ompA* interaction using native MicA, and a 'stabilized' MicA version ($MicA_{stab}$) modified to represent the structure of MicA in the *ompA*-binding site exposed conformation. Our data show that Hfq plays a multifaceted role in facilitating the MicA:*ompA* interaction. It causes both a change in structure in MicA and serves as a platform for both RNAs to bind. We further present data that at accumulated MicA levels, an Mg^{2+}-dependent self-association occurs. We discuss the potential impact of this Mg^{2+}-mediated effect.

MATERIALS AND METHODS

Hfq protein expression and purification

E. coli BL21 (DE3) cells containing the plasmid pEH-10(hfq), which encodes Hfq, were a kind gift from Dr I. Moll (Max F. Perutz Laboratories, University of Vienna, Austria). The cells were grown at 37°C in Luria Broth (LB) medium supplemented with 100 μg/μl of ampicillin, to an OD_{600} of 0.6. Protein expression was induced with 1 mM isopropyl β-D-1-thiogalactopyranoside (IPTG), and the cells were left to incubate for 3 h before harvesting by centrifugation (5000*g*, 20 min, 4°C). Hfq was purified as described by Vassilieva *et al.*, (20), except that after the hydrophobic interaction chromatography column, Hfq protein was concentrated with Sartorius VivaSpin 2 centrifugal concentrators (10 kDa molecular weight cut-off) and loaded onto a Superdex 200 10/300 size-exclusion column equilibrated in 20 mM Tris, pH 8, 500 mM NaCl, 0.5 mM ethylenediaminetetraacetic acid (EDTA) and 10% glycerol. Peak fractions were collected and concentrated as described earlier in the text to ~10 mg/ml before storing at −80°C. All Hfq concentrations relate to the protein in its hexameric form.

Preparation of RNAs

DNA templates encoding MicA, $MicA_{stab}$, DsrA sRNAs and the *ompA* leader (encoding −132 to +33) were generated through the extension of overlapping primers (21), with KOD hot start polymerase (Novagen). For *rpoS*, the plasmid *rpoS*-Blunt II TOPO (encoding −576 to +10 of *rpoS*) was used as template DNA. To generate this, *rpoS* (−576 to +10) was amplified from genomic DNA and ligated into a linearized pCR-Blunt II TOPO vector using the Zero Blunt® TOPO® polymerase chain reaction cloning kit (Invitrogen), (see Supplementary Table S1 for all primer sequences). Each sequence was designed to contain a T7 promoter sequence (5′-TAATA CGACTCACTATA) and up to three guanines at the 5′-end to enhance the yield from transcription. Analysis by Mfold indicated that these additional guanines would not be expected to interfere with the RNA structures formed. RNAs were transcribed *in vitro* by T7 RNA polymerase (Ambion Megascript kit) over 4 h. Template DNA was removed with TurboDNase, and the remaining RNA was purified (Ambion MegaClear kit). Some RNAs were radiolabelled at the 3′-end with [^{32}P]pCp (cytidine bis-phosphate) using T4 RNA ligase. Other RNAs were Cy labelled through the incorporation of 0.05 mM Cy3/5 uridine triphosphate (UTP) into the transcription reaction. Mfold was used to model RNA secondary structures (22).

Thermal melting of RNAs

Melting titrations of RNAs were carried out using 400 nM MicA or $MicA_{stab}$ in 10 mM Tris, pH 8.0, 50 mM NaCl and 50 mM KCl. Samples were measured in 0.5-cm path length quartz cuvettes with a lambda 35 spectrophotometer (Perkin Elmer). The absorbance was monitored at 260 nm from 20°C–95°C using a Peltier system, controlled by timedrive software (UVWINLAB).

Electrophoretic mobility shift assays (EMSAs)

RNAs were heated to 80°C for 2 min in 10 mM Tris, pH 8.0, 50 mM NaCl, 50 mM KCl, 0.5 mM EDTA and 10% v/v glycerol. For dimerization assays, 10 mM $MgCl_2$ was used in replacement of the EDTA. RNAs were then cooled for 5 min at room temperature (RT) to allow them to fold. All binding assays were carried out in 10 mM Tris, pH 8.0, 50 mM NaCl, 50 mM KCl and 10% v/v glycerol in 10 μl volumes. Reaction products were separated on 6% (w/v) native polyacrylamide gels (29:1 acrylamide:bis-acrylamide), run in 90 mM Tris, 90 mM borate, 2 mM EDTA (TBE) at 100 V for 1.5 h at 4°C. Cy5- and Cy3-labelled samples were analysed at 632 and 473 nm, respectively, and imaged with a Fujifilm imager (FLA-5000). Gels containing radiolabelled samples were imaged with a Fujifilm phosphoimager (FLA-5000) and analysed using MultiGuage software. Gels stained with SYBR Gold (Invitrogen) were visualized with a transilluminator.

Determination of ligand binding affinities

For RNA–RNA and Hfq–RNA interactions, the fraction of ^{32}P-labelled RNA in each RNA complex was calculated as a proportion of the total counts in each lane. MicA:*ompA*, $MicA_{stab}$:*ompA* and $MicA_{stab}$:Hfq were fitted to a single binding isotherm, whereas MicA:Hfq was fitted to a partition function for co-operative binding of Hfq to two independent sites, as described in Lease and Woodson (23) using Grafit 5 (Erithacus Software). The Hill coefficient, *n*, was 2. The concentrations of Hfq used in these experiments ranged from 0 to

100 nM (based on hexamer size; see Hfq protein expression and purification). At these concentrations, recent work by Panja and Woodson (24) suggests that Hfq would be monomeric [as their findings suggest that 166 nM Hfq (hexamer) or 1 μM Hfq (monomer) (24) is required for hexamer formation]. However, under the conditions used here, we observe the same mobility shift for MicA binding to Hfq at concentrations (based on hexamer size) above and below 166 nM (Supplementary Figure S1). Based on this, we conclude that the Hfq used in these experiments is in the hexameric form. The discrepancy of the lower stability of Hfq hexamer observed by Panja and Woodson (24) may potentially be explained by their introduction of a Cy label at Ser65, a location that has otherwise been implicated in impacting Hfq hexamer stability (25).

Size-exclusion chromatography and analytical ultracentrifugation

RNAs were heated to 80°C for 2 min and cooled at RT for 5 min in annealing buffer (10 mM Tris, pH 8.0, 50 mM KCl, 50 mM NaCl ± 10 mM $MgCl_2$). A volume (100 μl) of 1 μM of RNA was then applied to a Superdex 200 10/300 size-exclusion column equilibrated in the respective annealing buffer. Purified peaks were concentrated and were adjusted to three different concentrations (162, 362 and 638 nM for MicA; 167, 337 and 672 nM for DsrA). These were loaded into a six-channel centrepiece analytical ultracentrifugation (AUC) equilibrium cell, with reference buffer in the remaining three channels. Samples were sedimented with an Optima XL-A AUC (AnTi-50 eight hole rotor, Beckman Coulter), at 10 000 *g* for 24 h with a constant temperature of 10°C. Radial absorbance scans were measured at 265 nm after 18, 21 and 24 h. Proteomelab™ software was used to program the centrifuge and to record the data. Data were analysed using Origin software (Microcal Software Inc., developed by Beckman Coulter), whereby molecular weights were calculated using a partial specific volume for RNA of 0.53 ml/g.

Small angle X-ray scattering

Small angle X-ray scattering (SAXS) experiments were performed on the ID14-3 bioSAXs beamline at the European Synchrotron Radiation Facility (ESRF, Grenoble, France) with a wavelength of 0.931 Å and a camera length of 2.42 m, covering a Q range of 0.005–0.5 $Å^{-1}$ [where Q is the scattering vector ($4\pi\sin\theta/\lambda$)]. BsxCuBE software was used to acquire, record and process the raw data into 1D files. MicA/$MicA_{stab}$ and DsrA RNAs were buffer exchanged in to 10 mM Tris, pH 8.0, 50 mM NaCl and 50 mM KCl (± 10 mM $MgCl_2$) with Amicon Ultra 0.5 ml 10 k centrifugal concentrators. RNA samples were heated at 80°C for 2 min followed by 5 min at RT to allow them to fold. RNAs were centrifuged at 17 000*g* for 15 min before loading to ensure removal of any particulates. Data were collected at 25°C for three concentrations of each sample to overcome inter-particle effects and noise levels: $MicA_{stab}$ (1.19, 0.6 and 0.28 mg/ml), MicA dimer (1.16, 0.26 and 0.06 mg/ml), DsrA monomer (0.975, 0.6 and 0.28 mg/ml) and DsrA dimer (1.17, 0.76 and 0.28 mg/ml). The 10 × 10 s frames were acquired under a constant flow rate to avoid the effects of radiation damage. tRNA was used as a control to calculate molecular weight [MW of sRNA = I(0) sRNA/I(0) tRNA × MW of tRNA]. Scattering curves were buffer-subtracted and merged using Primus software (26). At low angles, the radius of gyration (R_g) was found using the Guinier approximation, $I(Q) = I(0) \exp {}^{1}/_{3} R_g^2 Q^2$. Transformation of the scattering curve by the GNOM program (27) generated a distribution of particle distances allowing the maximum dimension (D_{max}) to be determined. Confirmation of correct dimensions was achieved when the R_g from GNOM matched that obtained from the Guinier approximation. Dammif was used to make low resolution *ab inito* models (28). Twenty models were generated, averaged by Damaver and filtered with Damfilt to make a compact model that represented the most probable conformation (29).

Circular dichroism

Circular dichroism (CD) measurements were carried out on an Applied Photophysics π* − 180 spectrometer at 20°C. RNAs were heated for 2 min in 10 mM Tris, pH 8.0, supplemented with 0.5 mM EDTA for monomeric RNA formation or 10 mM Tris, pH 8.0, and 10 mM $MgCl_2$ for dimeric formation, before cooling at RT for 5 min. RNAs were buffer exchanged into 10 mM Tris, pH 8.0, 100 mM NaCl and Hfq into 20 mM Tris, pH 8.0, 500 mM NaCl with Micro BioSpin columns (Biorad). In all, 800 nM of RNA was measured with Hfq (hexamer) additions of 0, 800 nM and 1.6 μM. Measurements were then taken in a 0.4-mm path length over a wavelength range spanning 200–350 nm in 1-nm step sizes. The protein contribution was subtracted, and —four to six scans were averaged, baseline subtracted and smoothed using the Savitsky–Golay routine to reduce noise. The spectra were converted into molar ellipticity units ($deg\,cm^2\,dmol^{-1}$).

RESULTS

$MicA_{stab}$ as a tool to characterize MicA regulation

In isolation, MicA contains two stem loops at positions 26–46 nt (stem loop 1) and 54–71 nt (stem loop 2) in its native form (6). However, when MicA binds to the mRNA target, *ompA*, the structure is reorganized, such that stem loop 1 at position 26–46 nt is moved to position 34–52 nt (Figure 1a and b) (6). This switch is required to expose the *ompA*-binding site, which is partially blocked in the native MicA structure. To test the role of MicA structure in *ompA* regulation, a variant of MicA was designed to stabilize the '*ompA*-binding site exposed' conformation (hereafter referred to as $MicA_{stab}$). This was achieved by altering the nucleotides at positions 34–52 to include a high GC content so as to confine the stem loop to this location. The modified $MicA_{stab}$ secondary structure was predicted computationally by Mfold analysis (Figure 1c; altered nucleotides in bold).

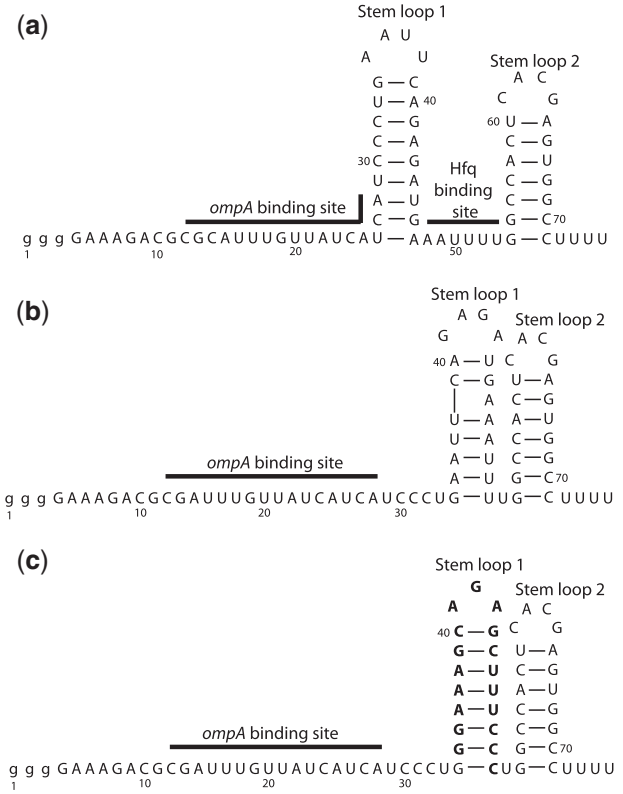

Figure 1. MicA conformations: native structure, *ompA*-bound and modified form ($MicA_{stab}$). (**a**) Native MicA structure with partially blocked accessibility to the *ompA*-binding site. (**b**) MicA structure when bound to *ompA* with the *ompA*-binding site exposed. (**c**) $MicA_{stab}$, a stabilized form of MicA with the *ompA*-binding site exposed, achieved by nucleotide substitution to increase the GC content within region 34–52 nt to stabilize the stem loop in this location. The nucleotides changed are indicated in bold. Experimentally verified structures in (a) and (b) were determined by Udekwu *et al.* (6); $MicA_{stab}$ was predicted by Mfold (22).

To demonstrate that the *ompA*-binding site is more exposed in $MicA_{stab}$ than in native MicA, *ompA* was incubated with increasing concentrations of either MicA or $MicA_{stab}$ (Figure 2a). It would be anticipated that $MicA_{stab}$ would bind *ompA* with higher affinity than MicA, as it has been designed to contain an accessible *ompA*-binding site, which is partially blocked in MicA. This was indeed seen to be the case, as the dissociation constant (K_d) for the $MicA_{stab}$:*ompA* interaction (20 nM) was identified as >6-fold tighter than that for MicA:*ompA* (190 nM). This demonstrated that the *ompA*-binding site was more accessible in $MicA_{stab}$ compared with MicA, and, therefore, that $MicA_{stab}$ likely incorporated the intended conformational change. Thermal melting profiles of both MicA and the $MicA_{stab}$ were also recorded (Figure 2b). These showed that $MicA_{stab}$ had a substantially higher T_m (67.5°C) than MicA (53.6°C), indicating that $MicA_{stab}$ is more stable, which is consistent with its increased content of base paired G–C in the relocated stem loop 1.

MicA forms oligomers

While working with MicA we noticed that it was able to self-associate, and that the level of self-association was strongly dependent on Mg^{2+} concentration [Figure 3a(i), left gel]. Although MicA oligomerization is Mg^{2+}-dependent, it was also found to be dependent on MicA concentration, with a MicA oligomerization K_d of 153 nM identified in the presence of 10 mM Mg^{2+} (Supplementary Figure S2a). Given that MicA expression is highly abundant in stationary phase (8), it is possible that local MicA concentrations, coupled with the physiologically relevant Mg^{2+} concentration of 10 mM (30), supports MicA oligomerization *in vivo*. However, in the absence of Mg^{2+}, MicA concentration had no effect on MicA-oligomeric state, with it maintaining monomeric form (Supplementary Figure S2a). Ca^{2+}, another divalent ion present in *E. coli* at ~90 nM (31) failed to impact the oligomeric state of MicA at physiologically relevant concentrations (Supplementary Figure S3). Additionally, Mn^{2+}, a divalent ion, which is often used in place of Mg^{2+}, did not produce the same MicA-oligomerization effect when tested in place of Mg^{2+} (data not shown). Interestingly, $MicA_{stab}$ lost the ability to oligomerize in an Mg^{2+}-dependent manner [Figure 3a(i), right gel], indicating that the MicA site of self-interaction depends on the native sequence within the 30–50 nt region of MicA, which has been modified in $MicA_{stab}$. As Mg^{2+} is a divalent ion known to support RNA folding, other sRNAs were also tested to explore whether this Mg^{2+}-dependent oligomerization occurs generally. DsrA, OxyS and RprA were tested, but only DsrA, an 87 nt sRNA involved in cold shock response and known to oligomerize from previous studies (32,33), predominantly formed a Mg^{2+}-dependent higher molecular weight species [Figure 3a(ii), upper gel]. Similar to MicA, DsrA oligomerization was also dependent on DsrA concentration with a DsrA oligomerization K_d of 235 nM identified in the presence of 10 mM Mg^{2+} (Supplementary Figure S2b). OxyS and RprA gave no evidence of Mg^{2+}-dependent oligomerization [Figure 3a(ii), middle and lower gels]. This shows the Mg^{2+}-dependent oligomerization phenomenon is sRNA specific.

Oligomer characterization

It was not possible from gel analysis to determine the oligomeric nature of the MicA and DsrA oligomers. However, previous studies (32–34) have indicated that DsrA is capable of oligomerizing into long fibres, but at the concentrations tested here, only one high molecular weight species was predominantly formed [Figure 3a(ii)]. Similarly, only one oligomeric MicA species was identified. Therefore, to identify the oligomeric state of these high molecular weight species, both MicA and DsrA oligomers were purified by size-exclusion chromatography and analysed by AUC sedimentation equilibrium analysis [Figure 3b(i) and c(i)]. This showed the high molecular weight species for MicA had a molecular weight of 42 069 Da (theoretical molecular weight of monomer is 24 997 Da), whereas the higher molecular weight species of DsrA had a molecular weight of 61 929 Da (theoretical molecular weight of monomer is 28 955 Da), both of which indicate that the high molecular weight species were dimeric forms of the sRNAs.

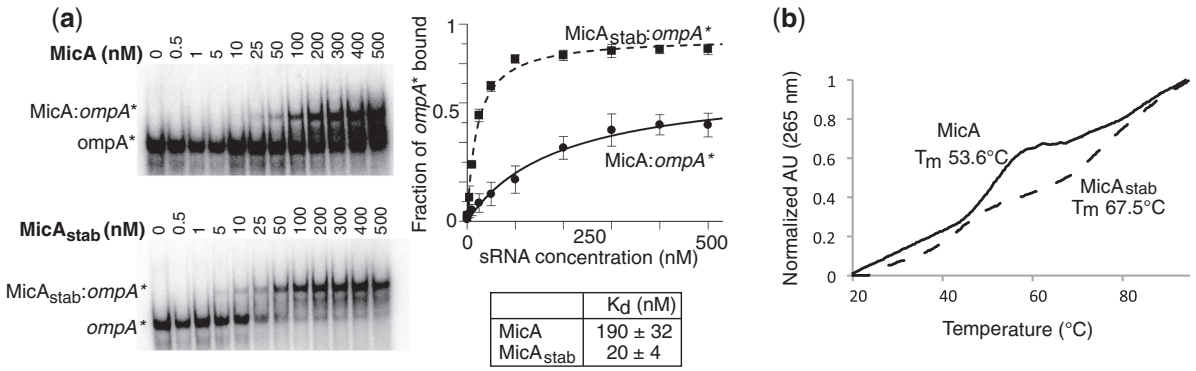

	K_d (nM)
MicA	190 ± 32
$MicA_{stab}$	20 ± 4

Figure 2. Comparison of MicA and $MicA_{stab}$. (**a**) EMSA of 5 nM ^{32}P *ompA** incubated for 30 min at 37°C with increasing concentrations of MicA (upper gel) or $MicA_{stab}$ (lower gel). The fraction of *ompA* bound is plotted as a function of sRNA concentration and shown graphically on the right, with MicA:*ompA* (solid line) and $MicA_{stab}$:*ompA* (dashed line). Standard errors of the mean are based on three experimental repeats. Data are fit to a single binding isotherm of the form Fraction Bound = [Total Bound × (sRNA)]/[K_d + (sRNA)]. The K_d for MicA:*ompA* and $MicA_{stab}$:*ompA* complexes are shown in the table below the graph. (**b**) Temperature melts of MicA (solid line) and $MicA_{stab}$ (dashed line). The normalized absorbance at 265 nm is plotted as a function of temperature (°C).

Furthermore, $MicA_{stab}$, identified as monomeric in the presence of Mg^{2+} [Figure 3a(i), right gel], was found to have a molecular weight of ~28 000 Da (theoretical MW of monomer is 24 568 Da) by AUC sedimentation velocity analysis (Supplementary Figure S4), further demonstrating $MicA_{stab}$ does not dimerize in the presence of Mg^{2+}, and thus indicating that the modified $MicA_{stab}$ sequence has disrupted the region involved in dimerization.

Additional evidence confirming that the high molecular weight DsrA and MicA species were dimeric was provided by SAXS analysis [Figure 3b(ii) and c(ii)]. $MicA_{stab}$, known to stay monomeric in the presence of Mg^{2+} [Figure 3a(i), right gel], had a radius of gyration (R_g) of 33.90 ± 0.01 Å with a maximum dimension (D_{max}) of 115 Å. In contrast, for MicA in the presence of Mg^{2+}, the R_g was 50.50 ± 0.01 Å with a D_{max} of 160 Å. Calculation of molecular weights using $tRNA_{Phe}$ as a standard indicated the $MicA_{stab}$ was 28 863 Da (close to monomeric weight), whereas the MicA species was 49 994 Da (close to dimeric weight). For DsrA, the R_g increased from 43.20 ± 0.02 to 53.30 ± 0.06 Å and the D_{max} increased from 160 to 185 Å in the presence of Mg^{2+}. In the absence of Mg^{2+}, the calculated molecular weight for DsrA was 29 054 Da, but when Mg^{2+} was added, this increased to 60 866 Da, again indicating the formation of a dimeric species. We saw no evidence for the formation of species of higher molecular weight than dimers in these experiments.

Collectively, these data show that Mg^{2+} causes MicA and DsrA to form dimers, and that the MicA dimerization site has been lost in $MicA_{stab}$. This suggests that the dimerization site is the region of MicA that is lacking in $MicA_{stab}$, i.e. the nucleotides in stem loop 1 of MicA (Figure 1a and c).

Dimerization site modelling

Computational sequence analysis using the oligo analysis tool at www.operon.com identified both MicA and DsrA as having large regions of near-perfect self-complementarity. Figure 3d(i) and (ii) show the models of MicA and DsrA dimer conformation from this analysis; with the predicted dimerization regions highlighted in pink. In comparison to MicA and DsrA, $MicA_{stab}$, RprA and OxyS sRNAs gave no evidence for regions of self-complementarity. This is consistent with the experimental findings that $MicA_{stab}$, RprA and OxyS did not form oligomers.

The DsrA dimerization region produced a maximum ΔG of −25.32 kcal/mol, whereas the MicA region was −38.09 kcal/mol (Oligo-analyser IDT technologies), both of which are more energetically favourable than the energies of the stem loops that occupy these regions under conditions of no Mg^{2+} (−18.64 kcal/mol for DsrA and −16.27 kcal/mol for MicA). The self-complementarity sequence obtained for DsrA agrees with a $DsrA_{39–60}$ construct that has previously been shown to maintain capacity for oligomerization (32). For MicA, the self-complementarity region was generated at position 27–47 nt. This region was predicted to be the site of dimerization, as the $MicA_{stab}$ construct (which is identical to MicA except for the modified stem loop 1 sequence; Figure 1a and c), lacked self-association ability (Figure 3a(i), right gel). Nevertheless, the possibility that the dimers form via an alternative interaction, for example, a Mg^{2+}-bound 'kissing complex' with limited base pairing and co-axial extension of RNA helix or non-canonical base pairing, cannot be ruled out (35).

Exploring the dimeric forms

Hfq has been shown to enhance sRNA–mRNA pairing for both MicA (Supplementary Figure S5) (6) and DsrA (36). However, sRNA–mRNA pairing can occur, albeit more slowly, in the absence of Hfq [Supplementary Figure S5 (15,23)]. This allows it to be possible to probe the accessibility of the mRNA-binding site within the sRNA dimer conformations by directly monitoring mRNA binding to the sRNA dimers. Specifically, the *ompA*-binding site in MicA [Figure 3d(i); highlighted by the black line] overlaps slightly with the region implicated in dimerization, whereas, in contrast, one of the best-

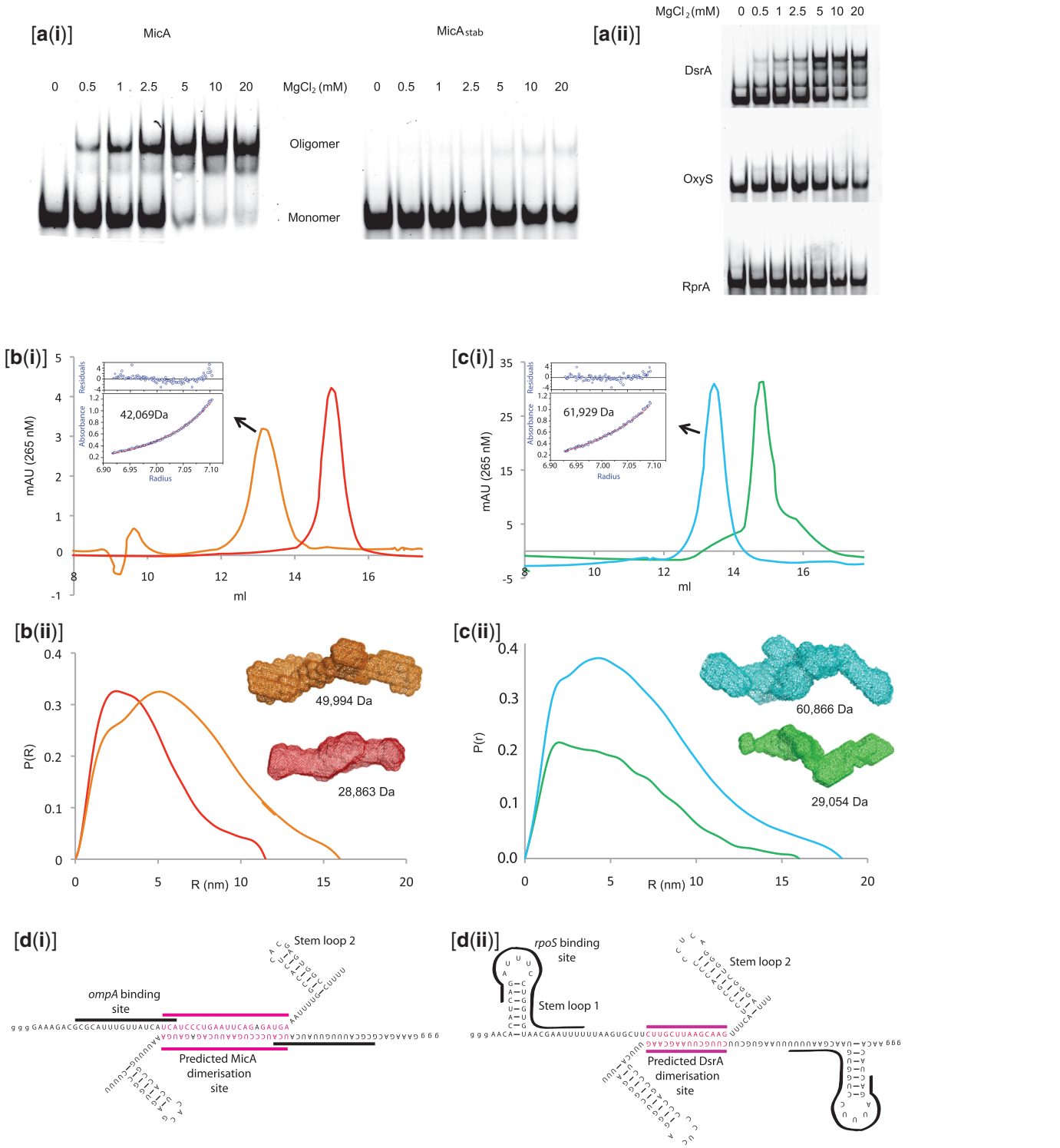

Figure 3. sRNA oligomerization. [**a**(i)] Native gel analysis of sRNAs in the presence of increasing concentrations of Mg^{2+}. 2 µM MicA (left gel) and $MicA_{stab}$ (right gel) were heated for 2 min at 80°C in 10 mM Tris, pH 8.0, 50 mM NaCl, 50 mM KCl, 10% glycerol with 0–20 mM Mg^{2+}. Two picomoles of each sample were analysed by 6% native polyacrylamide gel electrophoresis and stained with SYBR Gold. [a(ii)] As for [a(i)], but with sRNAs DsrA (top gel), OxyS (middle gel) and RprA (bottom gel). [**b**(i)] Size-exclusion chromatography profile monitoring RNA elution at 260 nm absorbance over time shows MicA without $MgCl_2$ (red) and with 10 mM $MgCl_2$ (orange). Inset shows AUC equilibrium analysis of the MicA species with 10 mM $MgCl_2$ (orange), which gave a molecular weight of 42 069 Da for the sample. [b(ii)] P(r) plots with corresponding *ab initio* models of $MicA_{stab}$ (red) and MicA (orange) with 10 mM $MgCl_2$. The molecular weights for each sample, calculated from the scattering data with $tRNA_{Phe}$ as a standard, are shown. [**c**(i) and c(ii)] As for b(i) and b(ii) respectively, but using DsrA without $MgCl_2$ (green) and with 10 mM $MgCl_2$ (blue). [**d**(i)] Model of MicA in dimer conformation. The pink lines and pink nucleotides highlight the predicted dimerization region. The complementary region for *ompA*-binding is highlighted by the black lines. [d(ii)] Model for DsrA in dimer conformation. Complementary regions for *rpoS* binding are highlighted by the black lines, whilst the pink lines and nucleotides highlight the region involved in DsrA dimerization.

characterized mRNA targets of DsrA, *rpoS*, binds to a region of the sRNA that is distinct to that of the site involved in dimerization [Figure 3d(ii)] (23). This would suggest a hypothesis that dimerization of MicA would impede *ompA*-binding, whereas the dimerization of DsrA would not affect its interaction with *rpoS*. Therefore, to assess whether the dimerization of MicA and DsrA influences their ability to interact with their mRNA targets, both the monomeric and dimeric forms of the sRNAs were incubated with their respective mRNA targets (*ompA* and *rpoS*, respectively) over time and analysed by EMSA (Figure 4). For the monomeric form of MicA, a clearly defined complex with *ompA* was displayed after ~2 min, with an initial binding rate of 0.9 nM/min (Figure 4a). For the dimeric form of MicA, the initial rate of binding to *ompA* was 13-fold slower than that of the monomer (0.07 nM/min), with no defined complex seen after 10 min (Figure 4a). This demonstrates that the *ompA*-binding site within MicA is indeed obstructed when the sRNA self-associates, as suggested by the dimerization site overlapping slightly with the *ompA*-binding site [Figure 3d(i)]. In contrast to MicA, the dimeric form of DsrA did not inhibit complex formation with *rpoS* (initial rate 1.5 nM/min), and the amount of complex formed was comparative with that observed for the DsrA monomer binding to *rpoS* (initial rate 1.0 nM/min; Figure 4b). This is similarly in agreement with the results available for DsrA that identified it to contain distinct regions for dimerization and *rpoS* binding [Figure 3d(ii)], thereby allowing both DsrA dimerization and interaction with *rpoS* to occur simultaneously. The self-association of DsrA, to form dimers, may 'loosen' the structure around the *rpoS*-binding site. This could account for the small increase in the initial binding rate observed for DsrA dimer:*rpoS*, compared to that seen for DsrA monomer:*rpoS*.

Monitoring structural changes in MicA monomer, MicA dimer and $MicA_{stab}$ upon Hfq addition

Hfq has been proposed to alter sRNA structure to mediate pairing with target mRNA (18). It is, therefore, possible that Hfq alters MicA monomer and MicA dimer structures, to form the *ompA*-binding site exposed conformation analogous to $MicA_{stab}$, such that it enables efficient pairing to *ompA*. *In vivo* findings of Udekwu *et al.* (6) show that Hfq is required for MicA-mediated downregulation of *ompA* and suggest that this is via Hfq aiding MicA-*ompA* pairing. Indeed, EMSA analysis, assessing the effect of Hfq on MicA-*ompA* pairing *in vitro*, confirmed the *in vivo* findings of Udekwu *et al.* (6), demonstrating that Hfq significantly enhanced the sRNA–mRNA interaction (Supplementary Figure S5). Hence, CD was performed to assess how the structural organization and oligomeric state of MicA affected the ability of Hfq to bind and change the sRNA's structure.

MicA monomer, $MicA_{stab}$ and MicA dimer were each measured by CD at a wavelength of 240–350 nm and then with a stepwise addition of Hfq hexamer. The protein

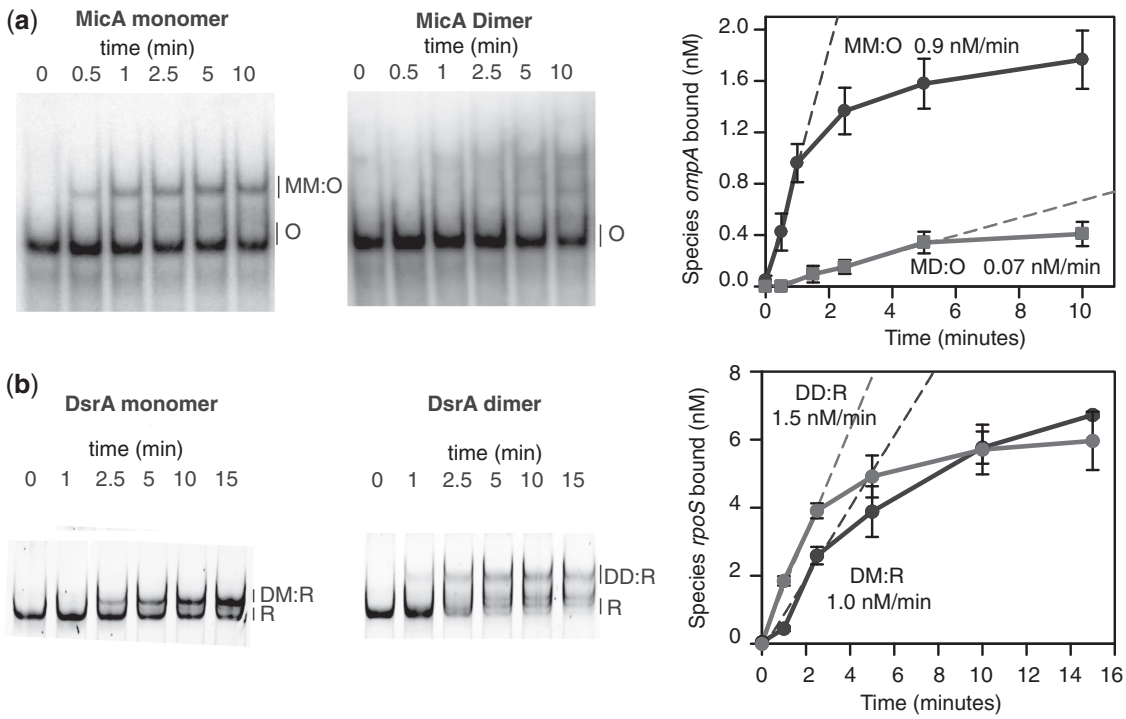

Figure 4. MicA and DsrA binding to their mRNA targets. (**a**) EMSA of 200 nM MicA monomer (left gel) or 200 nM MicA dimer (right gel) incubated with 10 nM ^{32}P *ompA** at 37°C, over time (indicated above the gel). Graphical representation of the data is shown on the right (solid lines) with the initial rates of degradation identified (dashed lines). Standard errors of the mean are based on three experimental repeats. (**b**) As for (a) but with 500 nM DsrA monomer or dimer incubated with 10 nM ^{32}P *rpoS**. Species are labelled with MM for MicA monomer, MD for MicA dimer, O for *ompA*, DM for DsrA monomer, DD for DsrA dimer and R for *rpoS*. The graphical representation of the complexes is shown as MM:O in black, MD:O in grey, DM:R in black and DD:R in grey.

contribution within the 240–350 nm region of the CD spectrum was subtracted, but because of the small number of aromatic residues within Hfq, this contribution was negligible. This means that the data at 240–350 nm showed only the contribution from the RNA. The ellipticity of the RNAs in the absence of Hfq and subsequently in the presence of increasing amounts Hfq was monitored until no further change in ellipticity was observed. Any ellipticity changes observed upon Hfq addition could be interpreted as indicating RNA conformational changes (37–39).

For MicA monomer, the maximal ellipticity change upon Hfq addition was reached at a MicA monomer:Hfq hexamer stoichiometric ratio of 1:2 with a 29% reduction in signal at 265 nm observed (i.e. from 1 to 0.7155 deg cm^2 $dmol^{-1}$; Figure 5a and Supplementary Figure S6a). The presence of two Hfq molecules binding to each MicA monomer was subsequently confirmed by EMSA (please see later in the text). By CD, this Hfq addition to MicA monomer was also observed to cause the width of the peak to narrow at 265–290 nm (Figure 5a and Supplementary Figure S6a), which can be interpreted as MicA monomer undergoing a structural rearrangement upon Hfq addition, potentially to expose the *ompA*-binding site and demonstrating Hfq functioning as an RNA chaperone. This was also supported by the observation that $MicA_{stab}$ (modified to represent MicA with the *ompA*-binding site revealed) did not display a peak narrowing at 265–290 nm upon Hfq addition (Figure 5b and Supplementary Figure S6b). It is possible that this lack of peak narrowing represents a lack of structural change in $MicA_{stab}$, as it is already in the structural conformation that Hfq would induce. Additionally, only a 20% maximal decrease in ellipticity was observed for Hfq addition to $MicA_{stab}$, and this was achieved at a 1:1 stoichiometric ratio of $MicA_{stab}$:Hfq hexamer (Figure 5b and Supplementary S6b) and can be interpreted as representing chromophore rearrangements due to quenching upon Hfq binding (38). Similar results were seen for MicA dimer (Figure 5c and Supplementary S6c), with a 20% decrease in ellipticity and with little change in the 265–290 nm range in terms of peak width upon Hfq addition. As MicA dimer and $MicA_{stab}$ display similar CD profiles upon Hfq addition, we can infer that the dimeric form of MicA allows Hfq to bind but prevents Hfq being able to alter the shape of the RNA in a means analogous to that seen for MicA monomer. Indeed, EMSA analysis showed that Hfq binds to the MicA dimer. However, it fails to disrupt the dimer conformation into the MicA monomer form (Supplementary Figure S7), which seems to be the form upon which Hfq can induce a structural change.

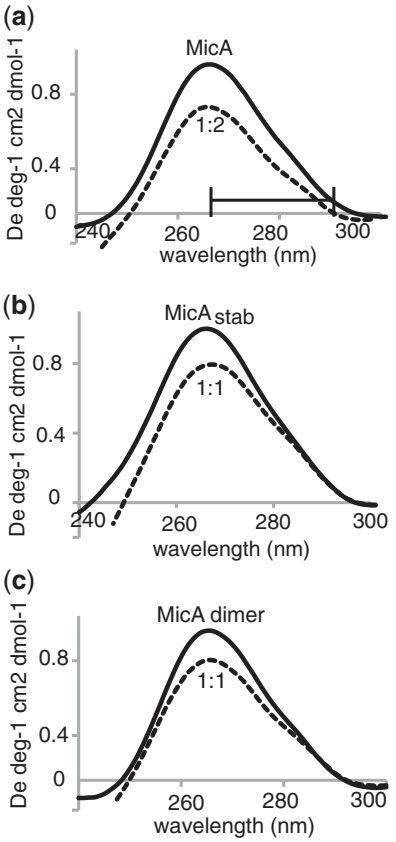

Figure 5. CD of MicA monomer, MicA dimer and $MicA_{stab}$ with Hfq. (**a**) CD spectra of 800 nM MicA monomer (solid line) and with 1600 nM Hfq hexamer (dashed line). The horizontal line highlights the 265–290 nm region of the profile discussed in the text. (**b**) Same as for (a) but for $MicA_{stab}$ (solid line) with 800 nM Hfq hexamer (dashed line). (**c**) Same as for (a) but for MicA dimer (solid line) with 800 nM Hfq hexamer (dashed line).

Comparison of MicA monomer, MicA dimer and $MicA_{stab}$ binding to Hfq and impact on ternary complex formation

MicA is known to contain one Hfq-binding site located between stem loops 1 and 2, encompassing ~47–53 nt (Figure 1a) (8). However, from our CD experiments, structural changes in MicA were seen up to a ratio of 1:2 MicA monomer:Hfq hexamer, indicating a second, as yet unidentified, Hfq-binding site exists within MicA. EMSAs confirmed this to be the case, as two distinct co-complexes were identified (Figure 6a), with the higher molecular weight species giving a Hill coefficient of $n = 2$, confirming that the species is 1:2 MicA:Hfq hexamer. The lower molecular weight species was, therefore, identified as a 1:1 MicA:Hfq hexamer complex. The K_d for the 1:1 complex was 2.3 nM (Figure 6a and c) and is in agreement with the findings of Fender *et al.* (40). However, the second Hfq-binding event to form the 1:2 complex had a weaker K_d of 65 nM (Figure 6a and c). In comparison, EMSAs of $MicA_{stab}$ with Hfq revealed only a tight 1:1 complex (K_d of 1.5 nM) to be formed (Figure 6b and c). This was in agreement with the CD experiments for $MicA_{stab}$, which displayed ellipticity changes only up to a ratio of 1:1 $MicA_{stab}$:Hfq hexamer, suggesting $MicA_{stab}$ to contain only one Hfq-binding site. Assessment of the predicted $MicA_{stab}$ secondary structure (by Mfold) shows it lacks the known Hfq-binding site between MicA stem loops 1 and 2 (Figure 1a and c). This accounts for the ability of $MicA_{stab}$ to bind only 1 Hfq hexamer. As $MicA_{stab}$ lacks the known Hfq-binding site and has similar affinities for Hfq as the 1:1 MicA:Hfq hexamer complex, it can be considered that these tight interactions with Hfq are located at the second unidentified site that

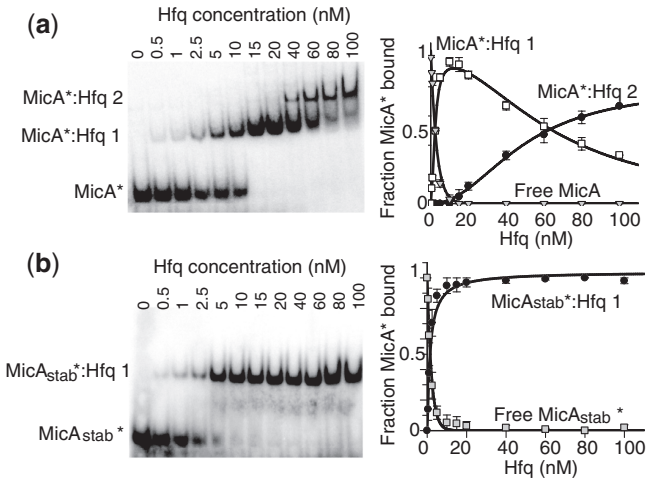

	K_d (nM)
MicA*-Hfq 1	2.3 ± 0.1
MicA*-Hfq 2	65 ± 2.9
$MicA_{stab}$*-Hfq 1	1.5 ± 0.2

Figure 6. Affinity of MicA/$MicA_{stab}$:Hfq complexes. Native EMSA of 5 nM ^{32}P labelled (**a**) MicA monomer* or (**b**) $MicA_{stab}$* mixed with increasing concentrations of Hfq hexamer. Samples were analysed by EMSA at RT (left, gel), and the fraction of bound species was plotted as a function of Hfq hexamer concentration (right, graph). Details of the graphical labels are as follows for the upper gel (a): MicA:Hfq 1 (white boxes), MicA:Hfq 2 (black spots), free MicA (grey triangles), whereas for the lower gel (b) are: $MicA_{stab}$:Hfq 1 (black spots) and free $MicA_{stab}$ (grey squares). MicA–Hfq was fit using a two-site partition model as per Lease and Woodson (23) giving $n = 2$. $MicA_{stab}$ was fit to a single binding isotherm. Standard errors of the mean are based on three experimental repeats. (**c**) Table showing the K_ds of the sRNA:Hfq complexes.

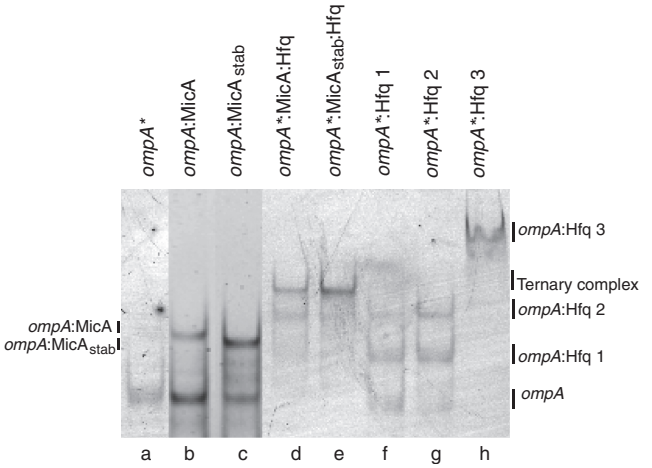

Figure 7. Ternary complexes of MicA/$MicA_{stab}$:*ompA*:Hfq. EMSA of (**a**) 10 nM Cy3 labelled *ompA**, (**b**) 10 nM *ompA* incubated with 200 nM MicA monomer, (**c**) 10 nM *ompA* incubated with 200 nM $MicA_{stab}$, (**d**) 10 nM Cy3 labelled *ompA** incubated with 200 nM MicA monomer plus 200 nM Hfq hexamer, (**e**) 10 nM Cy3 labelled *ompA** incubated with 200 nM $MicA_{stab}$ plus 200 nM Hfq hexamer, (**f**) 10 nM Cy3 labelled *ompA** incubated with 10 nM Hfq hexamer, (**g**) 10 nM Cy3 labelled *ompA** incubated with 20 nM Hfq hexamer and (**h**) 10 nM Cy3 labelled *ompA** incubated with 200 nM Hfq hexamer. All samples were analysed by 6% native polyacrylamide gel electrophoresis, on the same gel, at 4°C. Samples (b–c) were visualized for RNA with SYBR Gold and samples (a, d–h) were visualized for Cy3 labelled RNA by laser detection at 532 nm. A composite image of these differential visualizations of the same gel has been created. Constituents of the ternary complex were verified as shown in Supplementary Figure S8.

both MicA and $MicA_{stab}$ share. This second site could be involved in allowing the formation of a ternary complex comprising MicA:*ompA*:Hfq, which would facilitate the MicA:*ompA* interaction by bringing them into close proximity. This is supported by our observation, from EMSA analysis, that both MicA and $MicA_{stab}$ can form ternary complexes with *ompA* and Hfq, suggesting the two RNAs share the same Hfq-binding site within the context of ternary complex formation (Figure 7d and e and Supplementary Figure S8).

The weaker Hfq-binding event that occurs only for MicA and not $MicA_{stab}$ is presumably at the known binding site for Hfq on MicA, in the region between the stem loops 1 and 2 (47–53 nt) where the sRNA is structurally altered to allow release of the *ompA*-binding site. It would seem logical that Hfq binding to MicA in this region would bring about this structural rearrangement in the sRNA, and this is supported by our CD observations that a stoichiometric ratio of 1:2 MicA:Hfq hexamer is required to observe changes in the 265–290 nm region of the profile indicative of RNA structural changes. However, as a result of the Hfq-induced structural rearrangement of MicA, the weaker site to which the Hfq is bound would be lost, as it is sequestered into a stem loop that releases the *ompA*-binding site (Figure 1a and b). This would suggest that the Hfq bound at this region would, therefore, be displaced once the MicA structural change is complete and *ompA* can bind, and it is in agreement with this site having an observed weaker affinity for Hfq (30-fold weaker affinity compared with the tight 1:1 complex).

To explore whether there is recruitment of a second Hfq in the MicA:*ompA*:Hfq ternary complexes, EMSAs were used to determine whether one or two Hfq hexamers were present. As a marker of ternary complex stoichiometry, the $MicA_{stab}$:*ompA*:Hfq complex, in which $MicA_{stab}$ can only bind one Hfq, was run as a comparison. The band position of the MicA:*ompA*:Hfq complex was seen to be equal to that of the $MicA_{stab}$:*ompA*:Hfq complex, thereby identifying it to be in the same stoichiometric ratio (Figure 7). If two Hfq hexamers had been stably bound to MicA, a higher shift in the EMSA would have been observed. Therefore, although MicA can bind two Hfq hexamers, one of these is lost on ternary complex formation, potentially displaced after inducing the required MicA conformational change to allow *ompA*-binding. It is possible that the tightly binding Hfq (suggested to be responsible for the ternary complex formation) may also dissociate once the *ompA* and MicA have formed a stable duplex (although this is not seen here), as it may be RNA concentration driven, as suggested by Fender *et al.* (40).

DISCUSSION

For MicA to function as a negative regulator of translation of the target mRNA *ompA*, it is known that stem loop

1 must be rearranged closer to the 3′-end to free the *ompA*-binding site (Figure 1a and b) (6). Comparing native MicA to an artificially created stabilized version, in which the *ompA*-binding site was maintained in the exposed state ($MicA_{stab}$; Figure 1c), we have characterized MicA interactions.

One of the key findings of this study was the ability of MicA to self-interact. Although MicA concentration alone does not affect the sRNA's oligomeric state, we reveal that MicA is able to dimerize in an Mg^{2+}-dependent manner above a certain concentration of MicA. This could be expected as Mg^{2+} is a divalent cation that promotes interaction between two polyanionic RNAs, but this finding was not seen to be a general feature of all sRNAs, as RprA, OxyS and $MicA_{stab}$ were observed to be unaffected by the presence of Mg^{2+}. However, we also showed that the sRNA DsrA, which had been previously reported to form oligomers for unknown reasons (32–34), also specifically formed Mg^{2+}-dependent dimers above a certain DsrA concentration. DsrA dimerization results in minimal impact in terms of the ability of DsrA to pair, and upregulate, one of its main mRNA targets, *rpoS*. We note that a small enhancement of interaction rate is observed, potentially resulting from a minor destabilization of the stem loop at the *rpoS* interaction site, resulting from the downstream interaction of the paired DsrA molecules; although this remains unclear. More interestingly, however, although the region of DsrA dimerization does not directly impact the *rpoS* interaction site, it would in principle interfere with the binding of an alternative mRNA target, *H-NS* (41), which is downregulated in the presence of DsrA. Thus, DsrA dimerization could act as a means of coordinating mRNA binding preference.

By analogy to the DsrA dimer:*H-NS* situation, where the sRNA dimerization site overlaps with the mRNA target-binding site, the MicA dimerization site overlaps with the *ompA*-binding site. We show that the MicA dimer fails to pair to *ompA*, suggesting a potential additional means of mRNA regulation in which MicA dimerization results in the loss of function of MicA. Although current understanding of this potential regulatory mechanism is unknown, it is possible that MicA dimerization could target it for degradation. For example, the double-stranded RNA-specific endoribonuclease III cleaves *Salmonella typhimurum* MicA when it is paired to its target, *ompA* (9). Similarly, the double-stranded character of the MicA dimer could result in an analogous effect, resulting in enhanced cleavage of MicA, in dimer form, by RNase III. In contrast, RNase E is known to efficiently degrade free MicA, as in the absence of *ompA* pairing, or associated Hfq, it is vulnerable to attack (9,42). Dimerization of MicA could, therefore, act to block degradation by this single-stranded RNA-specific endoribonuclease. MicA dimerization could, therefore, act as a means of regulating the levels of functionally available MicA.

To further explore the potential relevance of the MicA dimer, it was necessary to consider the impact of Hfq. MicA dimer, MicA monomer and $MicA_{stab}$ were all seen to bind to Hfq. However, although Hfq was seen to be able to structurally affect MicA monomer, thereby demonstrating the chaperone function of Hfq, it was only able to bind, and not able to structurally affect, $MicA_{stab}$ or MicA dimer. As $MicA_{stab}$ is already in the correct conformation for *ompA* binding, it is not unsurprising that the $MicA_{stab}$ structure is not significantly affected by Hfq. In a similar way, the predicted MicA dimer structure has lost the stem loop occluding the *ompA*-binding site, which Hfq is proposed to melt. Hence, MicA dimer is also in the 'active' conformation for *ompA* binding, only in place of bound-*ompA*, a second MicA molecule has paired to MicA instead. Importantly, Hfq was not observed to induce dissociation of the MicA dimers into monomeric form, which seems to be required for MicA to function. Hence, the formation of MicA dimers seems to represent a means of inactivating MicA, with Hfq unable to restore the functional MicA monomer form. Consequently, in situations where MicA accumulates in the presence of Mg^{2+}, dimerization of MicA could potentially be seen to result in the 'switching off' of MicA function.

In addition to the MicA monomer structural changes that occur upon Hfq binding, MicA has been identified to bind to two Hfq hexamers. One Hfq-binding site has already been identified as being located between stem loops 1 and 2 (6). We have identified that this site has a 30-fold weaker affinity than the site at which the second Hfq binds. However, the location of this second Hfq binding site has not been identified. Previous work has shown that Hfq binds the 3′U-rich–end of the sRNA RybB (43). In addition, recent studies have further supported the 3′-end binding of Hfq to sRNAs by demonstrating that Hfq protects against 3′-end degradation by PNPase (44). The second Hfq-binding site observed for MicA could, therefore, be at the 3′U-rich–end of the sRNA. However, having multiple RNA-determinants involved in binding to a single Hfq hexamer has been demonstrated for the sRNA RybB (45). Consequently, this raises the possibility that although the 3′-end of MicA may well bind to Hfq, it could be a second determinant of the known site, with both sites binding to the same Hfq hexamer. Alternatively, the second Hfq hexamer observed to bind to MicA, could bind at a distinct, independent, location on MicA, and involve either single or multiple determinants. Internal U/A-rich regions of sRNAs (14), often adjacent to stem loops (46), or within the sRNA body (45) are known to be important in Hfq binding. Hence, the second Hfq-binding site within MicA could be located in such a region, and MicA nucleotides 15–23 present such an opportunity. Although this work has clearly identified that MicA can bind to two Hfq hexamers, and that two distinct binding events exist of differing affinities, further work is required to explore in detail the hypotheses raised here and fully characterize the MicA determinants of Hfq binding.

Although two Hfq hexamers are identified as binding to MicA, we find that only one Hfq hexamer remains bound upon ternary complex formation with *ompA*. Our data, therefore, supports a hypothesis that Hfq binding to MicA at the newly identified high affinity site could be involved in bringing the target transcript, *ompA*, into close proximity with MicA to aid pairing. A subsequent

Hfq–MicA binding event at the lower affinity site, proposed to be at the known binding site between step loops 1 and 2, is necessary to allow restructuring of MicA, such that the *ompA*-binding site becomes exposed. After MicA restructuring, the lower affinity Hfq-binding site is lost and the Hfq involved then dissociates. Upon exposure of the *ompA*-binding site within MicA, MicA–*ompA* pairing occurs. It would be anticipated that the tightly bound Hfq would be lost once a stable MicA–*ompA* duplex had formed, although this may be driven by RNA concentration (40) and was not seen in our experiments.

In summary, our studies to characterize the interactions of MicA have expanded our understanding of the sRNA's function. We have demonstrated Hfq's role as an RNA chaperone, impacting the structural conformation of MicA. We have seen that MicA is capable of binding to two Hfq hexamers and discuss a potential mechanism of MicA action which explains our observation of one Hfq hexamer within the context of a ternary complex with *ompA*. In addition, we have identified that a potentially inactive Mg^{2+}-dependent MicA dimer can form at accumulated MicA levels. Although it is well established that dimerization of proteins acts as a regulatory mechanism in signal transduction pathways (47) and RNA dimerization is an essential process in the retroviral replication cycle (48), dimerization has never before been identified as a potential means of regulating sRNA function. The capacity of sRNA dimerization to prevent interactions with specific mRNA targets, although continuing to allow interactions with others, provides a possible mechanism of sRNA-dimer driven mRNA-target preferences. This could potentially provide part of the explanation as to how one sRNA can specifically act on multiple mRNA targets. The ability of certain sRNAs to sense their environment, specifically in terms of ion levels, could suggest that a hitherto unknown level of regulation exists.

SUPPLEMENTARY DATA

Supplementary Data are available at NAR Online: Supplementary Table 1 and Supplementary Figures 1–8.

ACKNOWLEDGEMENTS

The authors thank Dr Isabella Moll (Max F. Perutz Laboratories, University of Vienna, Austria) for the kind gift of the *E. coli* Hfq expression strain. They thank Dave Whitley (University of Portsmouth) for help with binding equations. They thank Petra Pernot (European Synchrotron Radiation Facility, Grenoble, France) for SAXS technical support and Marc Malfois (Diamond Light source) for useful SAXS analysis discussions. They also thank Ben Luisi (University of Cambridge, UK) for critical reading of the manuscript.

FUNDING

BBSRC research grant [BB/F013140/1 to A.J.C.]; Marie Curie Reintegration Grant from the European Commission, FP7 [249154 to H.A.V.]; Institute of Biomedical and Biomolecular Science (IBBS), University of Portsmouth bursary (to C.A.H); European Synchrotron Radiation Facility beamtime access grants [MX-1226 and MX-1102 to A.J.C.]. Funding for open access charge: BBSRC research grant.

Conflict of interest statement. None declared.

REFERENCES

1. De Las Penas,A., Connolly,L. and Gross,C.A. (1997) The sigmaE-mediated response to extracytoplasmic stress in *Escherichia coli* is transduced by RseA and RseB, two negative regulators of sigmaE. *Mol. Microbiol.*, **24**, 373–385.
2. Ades,S.E., Connolly,L.E., Alba,B.M. and Gross,C.A. (1999) The *Escherichia coli* sigma(E)-dependent extracytoplasmic stress response is controlled by the regulated proteolysis of an anti-sigma factor. *Genes Dev.*, **13**, 2449–2461.
3. Alba,B.M., Leeds,J.A., Onufryk,C., Lu,C.Z. and Gross,C.A. (2002) DegS and YaeL participate sequentially in the cleavage of RseA to activate the sigma(E)-dependent extracytoplasmic stress response. *Genes Dev.*, **16**, 2156–2168.
4. Kabir,M.S., Yamashita,D., Koyama,S., Oshima,T., Kurokawa,K., Maeda,M., Tsunedomi,R., Murata,M., Wada,C., Mori,H. *et al.* (2005) Cell lysis directed by sigmaE in early stationary phase and effect of induction of the *rpoE* gene on global gene expression in *Escherichia coli*. *Microbiology*, **151**, 2721–2735.
5. Rhodius,V.A., Suh,W.C., Nonaka,G., West,J. and Gross,C.A. (2006) Conserved and variable functions of the sigmaE stress response in related genomes. *PLoS Biol.*, **4**, e2.
6. Udekwu,K.I., Darfeuille,F., Vogel,J., Reimegard,J., Holmqvist,E. and Wagner,E.G. (2005) Hfq-dependent regulation of OmpA synthesis is mediated by an antisense RNA. *Genes Dev.*, **19**, 2355–2366.
7. Johansen,J., Eriksen,M., Kallipolitis,B. and Valentin-Hansen,P. (2008) Down-regulation of outer membrane proteins by noncoding RNAs: unraveling the cAMP-CRP- and sigmaE-dependent CyaR-*ompX* regulatory case. *J. Mol. Biol.*, **383**, 1–9.
8. Rasmussen,A.A., Eriksen,M., Gilany,K., Udesen,C., Franch,T., Petersen,C. and Valentin-Hansen,P. (2005) Regulation of *ompA* mRNA stability: the role of a small regulatory RNA in growth phase-dependent control. *Mol. Microbiol.*, **58**, 1421–1429.
9. Viegas,S.C., Silva,I.J., Saramago,M., Domingues,S. and Arraiano,C.M. (2011) Regulation of the small regulatory RNA MicA by ribonuclease III: a target-dependent pathway. *Nucleic Acids Res.*, **39**, 2918–2930.
10. Schuppli,D., Georgijevic,J. and Weber,H. (2000) Synergism of mutations in bacteriophage Q beta RNA affecting host factor dependence of Q beta replicase. *J. Mol. Biol.*, **295**, 149–154.
11. Franze de Fernandez,M.T., Eoyang,L. and August,J.T. (1968) Factor fraction required for the synthesis of bacteriophage Qbeta-RNA. *Nature*, **219**, 588–590.
12. Link,T.M., Valentin-Hansen,P. and Brennan,R.G. (2009) Structure of *Escherichia coli* Hfq bound to polyriboadenylate RNA. *Proc. Natl Acad. Sci. USA*, **106**, 19292–19297.
13. Sauter,C., Basquin,J. and Suck,D. (2003) Sm-like proteins in Eubacteria: the crystal structure of the Hfq protein from *Escherichia coli*. *Nucleic Acids Res.*, **31**, 4091–4098.
14. Schumacher,M.A., Pearson,R.F., Moller,T., Valentin-Hansen,P. and Brennan,R.G. (2002) Structures of the pleiotropic translational regulator Hfq and an Hfq-RNA complex: a bacterial Sm-like protein. *EMBO J.*, **21**, 3546–3556.
15. Soper,T.J. and Woodson,S.A. (2008) The *rpoS* mRNA leader recruits Hfq to facilitate annealing with DsrA sRNA. *RNA*, **14**, 1907–1917.
16. Updegrove,T., Wilf,N., Sun,X. and Wartell,R.M. (2008) Effect of Hfq on RprA-*rpoS* mRNA pairing: Hfq-RNA binding and the influence of the 5′ *rpoS* mRNA leader region. *Biochemistry*, **47**, 11184–11195.

17. Geissmann,T.A. and Touati,D. (2004) Hfq, a new chaperoning role: binding to messenger RNA determines access for small RNA regulator. *EMBO J.*, **23**, 396–405.
18. Soper,T.J., Doxzen,K. and Woodson,S.A. (2011) Major role for mRNA binding and restructuring in sRNA recruitment by Hfq. *RNA*, **17**, 1544–1550.
19. Zhang,A., Wassarman,K.M., Ortega,J., Steven,A.C. and Storz,G. (2002) The Sm-like Hfq protein increases OxyS RNA interaction with target mRNAs. *Mol. Cell*, **9**, 11–22.
20. Vassilieva,I.M., Rouzanov,M.V., Zelinskaya,N.V., Moll,I., Blasi,U. and Garber,M.B. (2002) Cloning, purification, and crystallization of a bacterial gene expression regulator—Hfq protein from *Escherichia coli*. *Biochemistry (Mosc.)*, **67**, 1293–1297.
21. Gao,X., Yo,P., Keith,A., Ragan,T.J. and Harris,T.K. (2003) Thermodynamically balanced inside-out (TBIO) PCR-based gene synthesis: a novel method of primer design for high-fidelity assembly of longer gene sequences. *Nucleic Acids Res.*, **31**, e143.
22. Zuker,M. (2003) Mfold web server for nucleic acid folding and hybridization prediction. *Nucleic Acids Res.*, **31**, 3406–3415.
23. Lease,R.A. and Woodson,S.A. (2004) Cycling of the Sm-like protein Hfq on the DsrA small regulatory RNA. *J. Mol. Biol.*, **344**, 1211–1223.
24. Panja,S. and Woodson,S.A. (2012) Hexamer to monomer equilibrium of *E. coli* Hfq in solution and its impact on RNA annealing. *J. Mol. Biol.*, **417**, 406–412.
25. Vincent,H.A., Henderson,C.A., Ragan,T.J., Garza-Garcia,A., Cary,P.D., Gowers,D.M., Malfois,M., Driscoll,P.C., Sobott,F. and Callaghan,A.J. (2012) Characterization of *Vibrio cholerae* Hfq provides novel insights into the role of the Hfq C-terminal region. *J. Mol. Biol.*, **420**, 56–69.
26. Konarev,P.V., Volkov,V.V., Sokolova,A.V., Koch,M.H.J. and Svergun,D.I. (2003) PRIMUS: a windows PC-based system for small-angle scattering data analysis. *J. Appl. Cryst.*, **36**, 1277–1282.
27. Svergun,D.I. (1992) Determination of the regularization parameter in indirect-transform methods using perceptual criteria. *J. Appl. Cryst.*, **25**, 495–503.
28. Franke,D. and Svergun,D.I. (2009) DAMMIF, a program for rapid *ab-initio* shape determination in small-angle scattering. *J. Appl. Cryst.*, **42**, 342–346.
29. Volkov,V.V. and Svergun,D.I. (2003) Uniqueness of *ab initio* shape determination in small-angle scattering. *J. Appl. Cryst.*, **36**, 860–864.
30. Hurwitz,C. and Rosano,C.L. (1967) The intracellular concentration of bound and unbound magnesium ions in *Escherichia coli*. *J. Biol. Chem.*, **242**, 3719–3722.
31. Gangola,P. and Rosen,B.P. (1987) Maintenance of intracellular calcium in *Escherichia coli*. *J. Biol. Chem.*, **262**, 12570–12574.
32. Cayrol,B., Geinguenaud,F., Lacoste,J., Busi,F., Le Derout,J., Pietrement,O., Le Cam,E., Regnier,P., Lavelle,C. and Arluison,V. (2009) Auto-assembly of *E. coli* DsrA small noncoding RNA: molecular characteristics and functional consequences. *RNA Biol.*, **6**, 434–445.
33. Cayrol,B., Nogues,C., Dawid,A., Sagi,I., Silberzan,P. and Isambert,H. (2009) A nanostructure made of a bacterial noncoding RNA. *J. Am. Chem. Soc.*, **131**, 17270–17276.
34. Busi,F., Cayrol,B., Lavelle,C., LeDerout,J., Pietrement,O., Le Cam,E., Geinguenaud,F., Lacoste,J., Regnier,P. and Arluison,V. (2009) Auto-assembly as a new regulatory mechanism of noncoding RNA. *Cell Cycle*, **8**, 952–954.
35. Ennifar,E., Walter,P., Ehresmann,B., Ehresmann,C. and Dumas,P. (2001) Crystal structures of coaxially stacked kissing complexes of the HIV-1 RNA dimerization initiation site. *Nat. Struct. Biol.*, **8**, 1064–1068.
36. Sledjeski,D.D., Whitman,C. and Zhang,A. (2001) Hfq is necessary for regulation by the untranslated RNA DsrA. *J. Bacteriol.*, **183**, 1997–2005.
37. Tan,R. and Frankel,A.D. (1992) Circular dichroism studies suggest that TAR RNA changes conformation upon specific binding of arginine or guanidine. *Biochemistry*, **31**, 10288–10294.
38. Aparicio,F., Vilar,M., Perez-Paya,E. and Pallas,V. (2003) The coat protein of prunus necrotic ringspot virus specifically binds to and regulates the conformation of its genomic RNA. *Virology*, **313**, 213–223.
39. Daly,T.J., Rusche,J.R., Maione,T.E. and Frankel,A.D. (1990) Circular dichroism studies of the HIV-1 Rev protein and its specific RNA binding site. *Biochemistry*, **29**, 9791–9795.
40. Fender,A., Elf,J., Hampel,K., Zimmermann,B. and Wagner,E.G. (2010) RNAs actively cycle on the Sm-like protein Hfq. *Genes Dev.*, **24**, 2621–2626.
41. Lease,R.A. and Belfort,M. (2000) A trans-acting RNA as a control switch in *Escherichia coli*: DsrA modulates function by forming alternative structures. *Proc. Natl Acad. Sci. USA*, **97**, 9919–9924.
42. Bandyra,K.J., Said,N., Pfeiffer,V., Gorna,M.W., Vogel,J. and Luisi,B.F. (2012) The seed region of a small RNA drives the controlled destruction of the target mRNA by the endoribonuclease RNase E. *Mol. Cell*, **47**, 943–953.
43. Sauer,E. and Weichenrieder,O. (2011) Structural basis for RNA 3′-end recognition by Hfq. *Proc. Natl Acad. Sci. USA*, **108**, 13065–13070.
44. Andrade,J.M., Pobre,V., Matos,A.M. and Arraiano,C.M. (2012) The crucial role of PNPase in the degradation of small RNAs that are not associated with Hfq. *RNA*, **18**, 844–855.
45. Sauer,E., Schmidt,S. and Weichenrieder,O. (2012) Small RNA binding to the lateral surface of Hfq hexamers and structural rearrangements upon mRNA target recognition. *Proc. Natl Acad. Sci. USA*, **109**, 9396–9401.
46. Moll,I., Afonyushkin,T., Vytvytska,O., Kaberdin,V.R. and Blasi,U. (2003) Coincident Hfq binding and RNase E cleavage sites on mRNA and small regulatory RNAs. *RNA*, **9**, 1308–1314.
47. Klemm,J.D., Schreiber,S.L. and Crabtree,G.R. (1998) Dimerization as a regulatory mechanism in signal transduction. *Annu. Rev. Immunol.*, **16**, 569–592.
48. Baig,T.T., Lanchy,J.M. and Lodmell,J.S. (2007) HIV-2 RNA dimerization is regulated by intramolecular interactions *in vitro*. *RNA*, **13**, 1341–1354.